Supporting Information

Quantitative Assessment of Vapor Molecule Adsorption to Solid Surfaces by Flow Rate Monitoring in Microfluidic Channels

Faramarz Hossein-Babaei*, Ali Hooshyar Zare, and Mohsen Gharesi

Electronic Materials Laboratory, Electrical Engineering Department, K. N. Toosi University of Technology, Tehran, 16317-14191, Iran. *E-mail: fhbabaei@kntu.ac.ir; fhbabaei@yahoo.com

Contents:

S1. Microchannel fabrication

Various substrates are utilized for the fabrication of microchannels. For bulk materials testing, the microchannels are made using the standard techniques, such as molding, machining, etching, laser engraving, and 3D printing. Our PMMA microchannels, presented here as an example (see Figure 1), are made by CO_2 laser engraving: PMMA sheets with 2 mm thickness are cut into 50 mm × 6 mm slabs using a continuous wave CO_2 laser. The microchannel is formed by the engraving mode of the laser at a lower laser power. The CO_2 laser machine and an engraved PMMA slab are shown in Figure S1.

In this method, a 25 μm deep trench with 50 mm × 4 mm dimensions is formed on each PMMA slab. The laser beam has a focus spot diameter of 80 μm, which is scanned over the slab for trench formation. The trench depth is controlled by the traveling speed and output power of the laser beam and is measured using a standard screw gauge micrometer. The speed and power chosen for channel formation on PMMA are 200 $mm.s^{-1}$ and 8 W, respectively. Engraved slabs are polished, washed with absolute ethanol and distilled water in an ultrasonic bath and left to dry at room temperature. Finally, two trenched slabs are bonded together using the SATB technique described in reference [50] to form a 50 μm deep microchannel. The method involves pressing the two slabs together and chloroform injection to their interface at 50 °C.

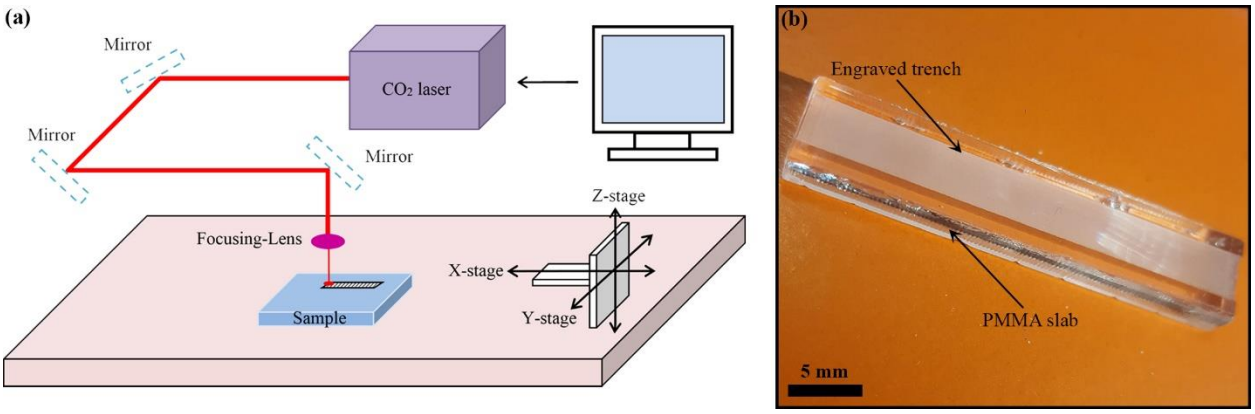

Figure S1. Schematic presentation of the CO_2 laser machine utilized for microchannel fabrication (a) and the photograph of a PMMA slab with a laser engraved micro-trench (b).

Au- and ZnO-coated microchannels are fabricated by depositing the coating material on the engraved PMMA slabs prior to the SATB process. Au coatings are formed by the sputter-deposition of 20 nm-thick Au films on the PMMA slabs in Ar atmosphere with a pressure of 1 Pa. ZnO coatings are produced by drop-casting a 10 mM aqueous ZnO suspension, followed by air drying at 50 °C for 30 min. The resulting ZnO layers are 5 μm thick. For forming ZnO microchannels, slightly deeper trenches are formed on the PMMA slabs to compensate for the extra thickness of the ZnO layers. All the examined microchannels have depths in the 45-55 μm range.

More recently, we utilize the facile and fast method of spacing-bonding (SB) for channel fabrication. In this method, a spacer with a thickness equal to the desired channel depth is placed between the unprocessed slabs. Then the two slabs are pressed together for bonding and channel formation. SB method has the advantage of maintaining the initial form of the surface during the microchannel fabrication process as the engraving and polishing steps are omitted. The method is schematically illustrated in Figure S2. Further simplification of the method is achieved by utilizing the common double-sided tapes with 50 μm thickness as the spacer. After attaching one side to the whole area of slab-1, the tape is laser cut to the desired shape. Then, the slab-2 is pressed to the slab-1 for channel formation after the selective removal of the laser delineated tape. In this method, the double-sided tapes function both as the spacer and the bonding agent. Figure S3 shows microchannels with different shapes and geometries produced by this technique. For fabricating coated microchannels, the coating processes, such as those described in the previous paragraph, are performed on PMMA slabs prior to the SB process. By the use of SB method for channel formation, the gas adsorption experiments reflect the actual adsorption coefficient of the material in its applied form as no surface modifying processes such as polishing, etching, or engraving is carried out.

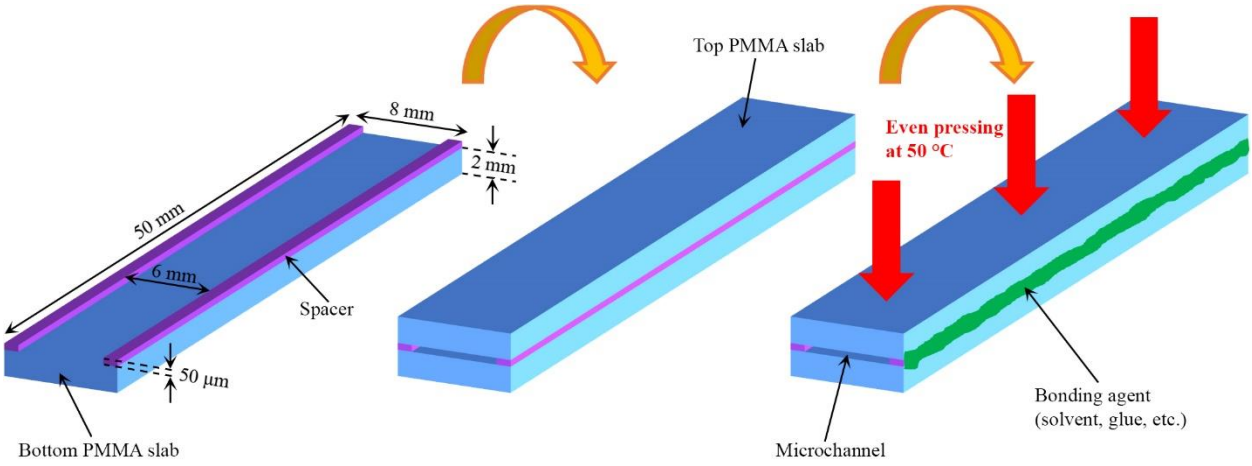

Figure S2. Schematic illustration of the SB technique employed for microchannel fabrication.

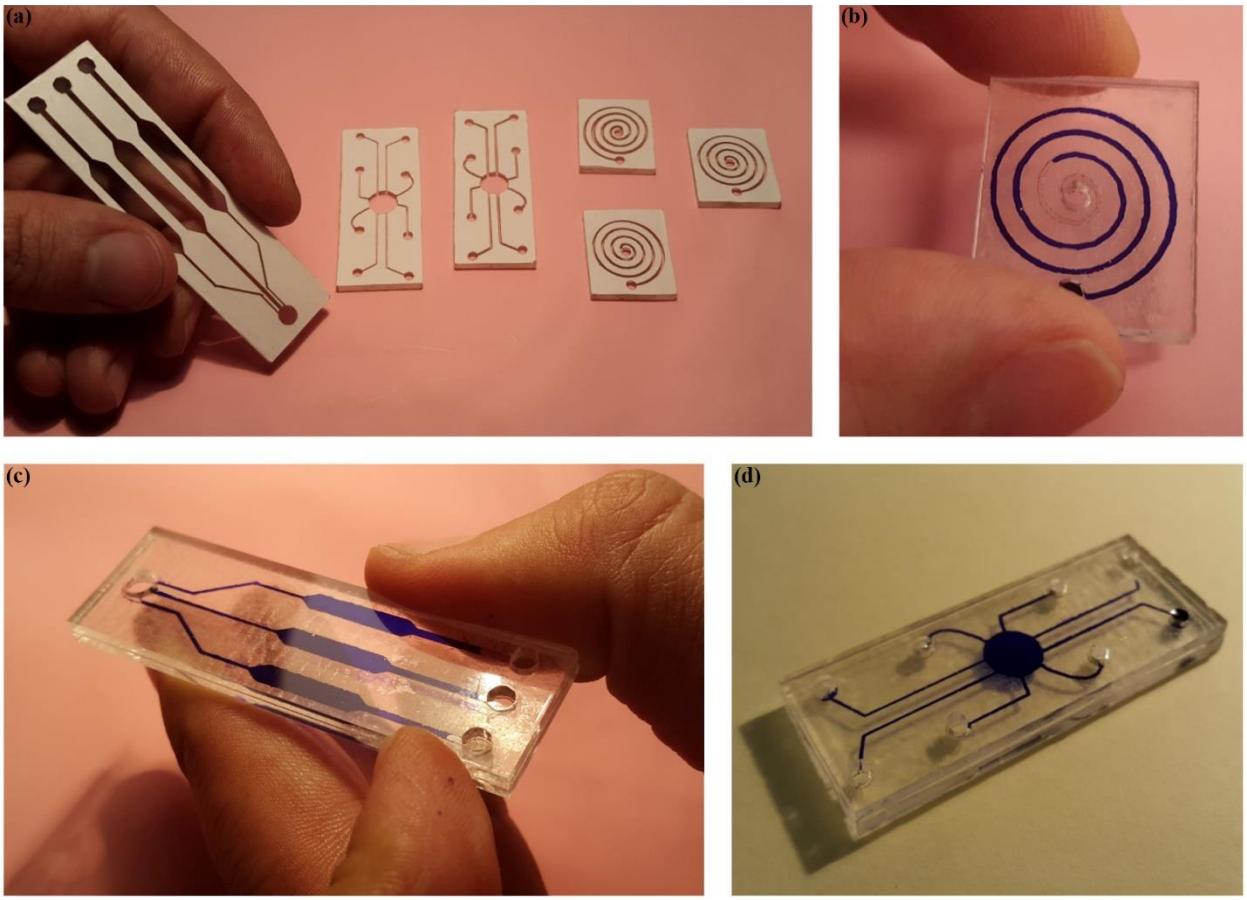

Figure S3. Microchannel fabrication by the modified SB technique; **(a)** photograph of the PMMA slabs with laser-delineated double-sided tapes, **(b-d)** the fabricated microchannels filled with blue ink for clarity.

S2. Sensor cavity

The microchannel made out of the material under test is butt joint to the microcavity. The cavity is reusable, and the butt joint created using Teflon tape can easily be replaced for different test channels. The cavity is made of aluminum by CNC discharge milling machine; the structure is presented in Figure S4a. The analyte concentration inside the microcavity is monitored using a low-cost commercial tin oxide-based gas sensor (SP3-AQ2, FIS Inc., Japan) which has general sensitivity to various air pollution sources, e.g., VOCs, H_2S, H_2, CO, etc., and an ethanol detection limit of 1 ppm in air, as per the sensor datasheet. The photograph of the sensing pellet of the device is shown in Figure S4b, demonstrating its 1.2 mm diameter SnO_2 pellet standing on a 2.0 mm x 2.0 mm x 0.3 mm alumina chip. After removing its polymer encapsulation, the sensor is embedded inside the microcavity, so that the sensing pellet of the sensor stands against the microchannel end. The sensor base is firmly cemented to the aluminum housing, and the lead wires providing power required for the sensor operation and response reading are connected to the outside electronic circuitry.

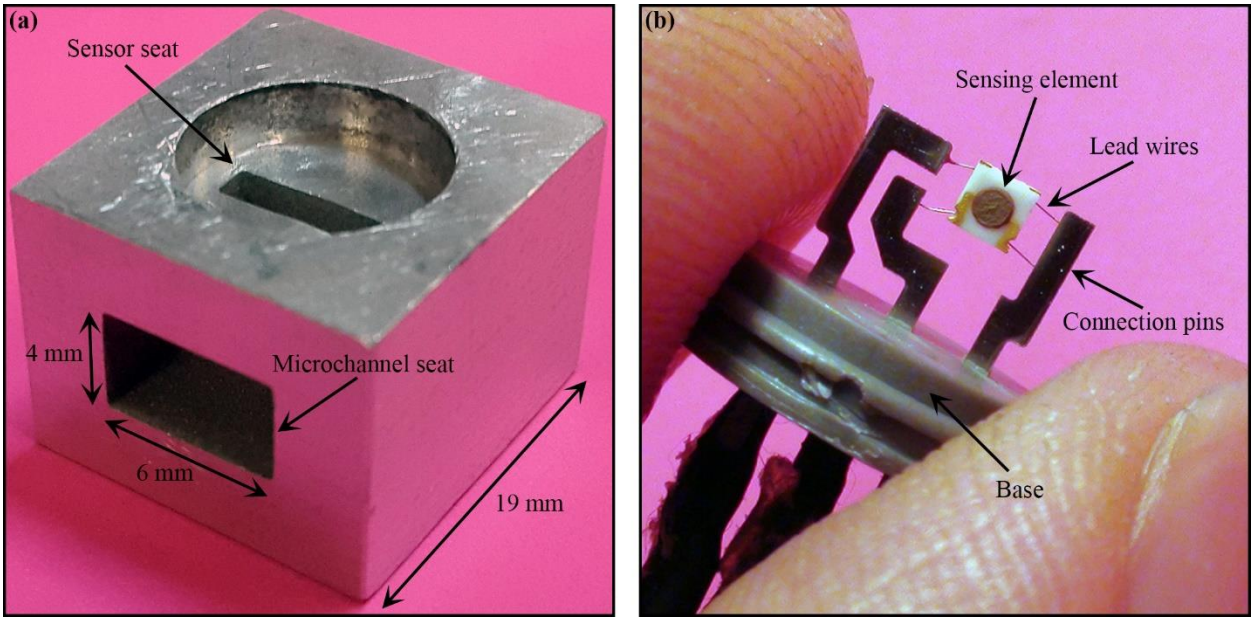

Figure S4. The microcavity made for housing the microchannel end and the gas sensor (a) and the sensor used for monitoring analyte concentration inside the microcavity (b).

S3. The measurement system

The experimental setup used for the recording of the data related to the gas adsorption-diffusion through the microchannel is schematically illustrated in Figure S5. It consists of an 8-L test chamber enclosed in a 64-L outer (reference) chamber. Both chambers are of cubic geometry and are made of laser-cut PMMA sheets cemented together using SATB technique. The whole system operates at isostatic condition; this is ensured by providing 1 mm diameter holes on the walls of both the inner and outer chambers which equalize the pressures in the chambers and the laboratory atmospheres. Considering the large volume of the outer chamber, the diffusion of the target molecules from the inner chamber to the outer chamber during each experiment (maximum of 15 min) is negligible. The "exhaust" hole provided on the microcavity housing the sensor has also a vital role in the isostatic performance of the system. Without these holes, the results recorded are irreproducible (see Section S6).

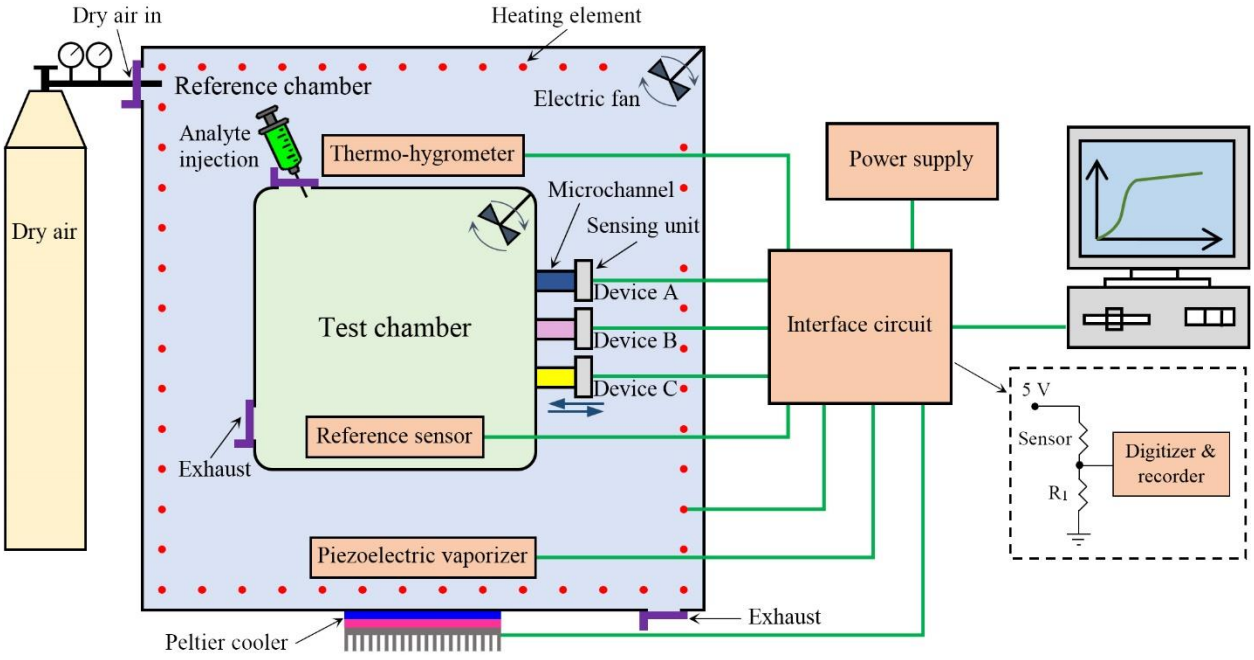

Figure S5. Schematics of the experimental setup used for measuring microchannel-analyte interactions; the inset shows the circuit diagram of the response measurement unit.

Prior to each test, both chambers are of clean air atmospheres; the relative humidity (RH) levels are controlled at 20 ± 4% range and both temperatures are at 26 ± 0.5 °C. These parameters are monitored using a calibrated thermo-hygrometer. The humidity level is decreased by the flow of dry synthetic air and is increased using a piezoelectric vaporizer installed inside the reference chamber. The latter facility is utilized when the experiment involves adsorption tests at high RH levels. The temperature is controlled by using Ni-Cr wire heater distributed on all the outer chamber walls. The outer chamber is also equipped with a Peltier cooler allowing gas adsorption tests at ambient temperatures as low as 10 °C.

Target molecules concentration levels are in the 500-1000 ppm (V/V) range. These concentration levels are prepared by injecting predetermined volumes of the target molecule to the inner (test) chamber. The outer chamber maintains its clean air atmosphere throughout the test. Uniform VOC distribution in the test chamber is guaranteed by the mild agitations provided by a small electric fan installed inside. The sensor installed at the microchannel end is electrically connected to the electronic interface unit which supplies power to the sensor and acquires responses in the form of voltage waveforms. The obtained response waveform is digitized and fed to the computer for processing. The developed system can simultaneously record the response patterns of 3 different microchannels.

S4. Preparing atmosphere with predetermined target molecule concentration

The result of adsorption parameter estimation using the presented method is almost insensitive to the actual contamination level in the test chamber. This is a major advantage of the presented method and stems from the fact that the adsorption parameters are extracted from the recorded response progress rates rather than the recorded response levels. Actually, prior to mathematical processing, all the recorded response patterns are amplitude normalized, and all cover the 0-1 response level range. However, due to the sensor nonlinearity (see Section S5), more reproducibility and higher precision in comparative assessments are achieved upon keeping approximately the same concentration level of the target molecule in the test chamber at different runs. This concentration level is predetermined based on the sensitivity level of the utilized sensor to the target molecule. For the VOC molecules, the concentration level in the test chamber

is around 1000 ppm, while the same for hydrogen is 500 ppm. The process of providing these concentration levels is described in the following paragraphs.

Liquid analytes, such as methanol, ethanol, and acetone, are introduced to the test chamber by a standard liquid microsampler. The microsampler head touches a small platform inside the chamber to ensure precise delivery. Time is allowed for the total evaporation of the liquid material within the chamber at room temperature. The evaporation and even distribution of the target molecule are assisted by the miniature electric fan installed within the chamber. The target molecule concentration build-up in the test chamber is monitored during the evaporation process; a steady level signal from the reference sensor indicates completion of the evaporation and distribution process. The process is schematically illustrated in Figure S6. The required volume of the liquid analyte, V_A, measured in μL, is calculated as follows:

$$V_A = \frac{C \times P \times V_C \times M_A}{D_A \times T \times R \times 10^9} \qquad \text{(S1)}$$

wherein, C is the desired analyte concentration in the test chamber stated in volume ppm, P is the atmospheric pressure stated in atm, V_C is the volume of the test chamber stated in mL, M_A is the molar mass of the target molecule in $g.mol^{-1}$, D_A is the density of the target molecule in its liquid state in $g.mL^{-1}$, T is the absolute temperature, and R is the universal gas constant 8.2×10^{-5} $m^3.atm.K^{-1}.mol^{-1}$. According to (S1), injecting 19.2 μL of ethanol to the test chamber creates an ethanol contamination level of 1000 ppm in the test chamber.

Gaseous analytes, such as H_2 and CO, are injected to the test chamber in specified volumes using gas tight syringes. Time (5 min) is allowed for the even distribution of the target molecules within the chamber, which is assisted by the miniature electric fan installed inside the chamber (see Figure S6). Considering the small volume of the injected gas compared to the test chamber volume, the target molecule concentration in the test chamber is calculated by dividing the injected volume to the volume of the test chamber. The reference sensor installed within the chamber monitors the target molecule concentration level during the experiment.

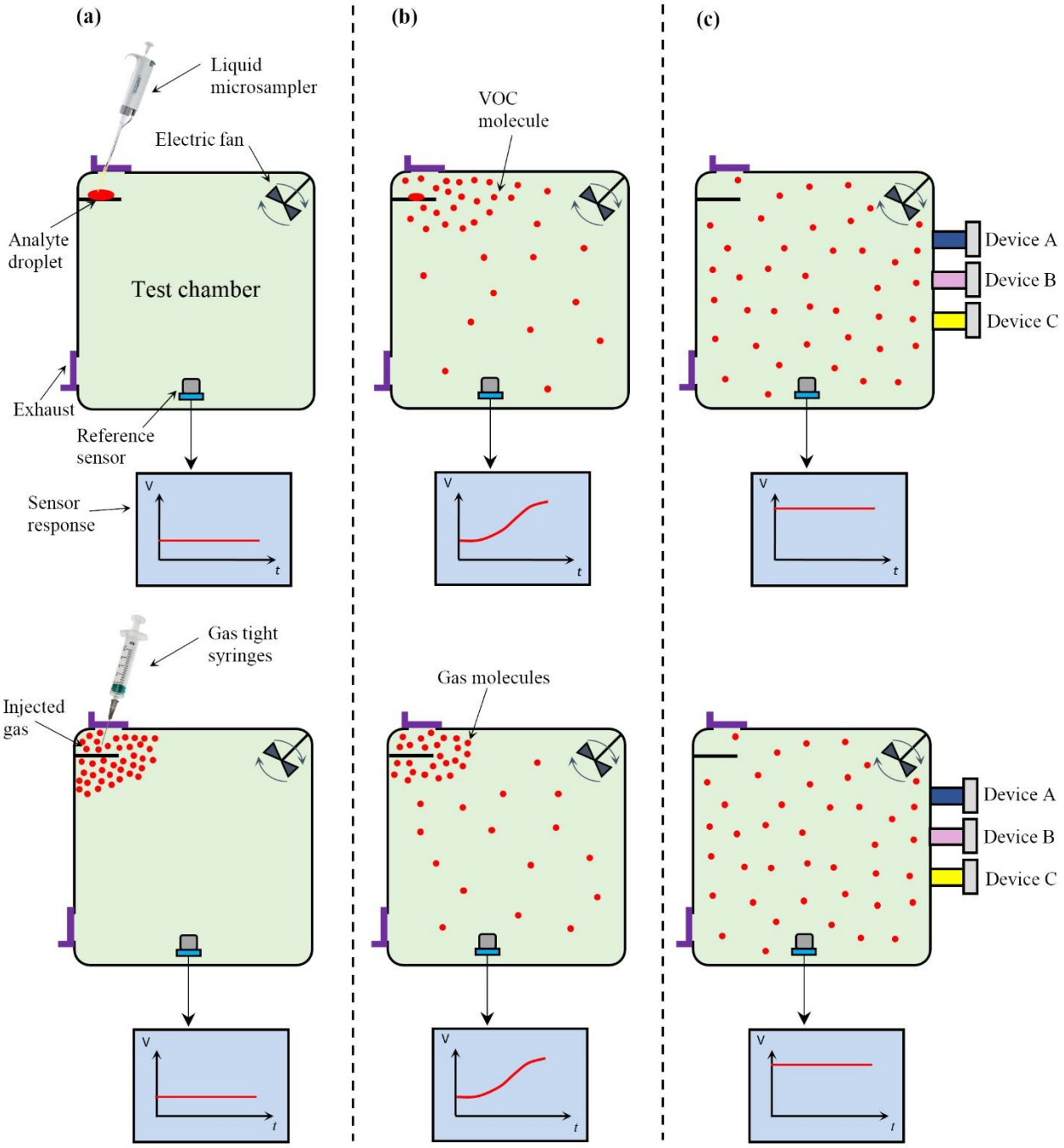

Figure S6. Schematic demonstration of the steps for creating predetermined target molecule concentration inside the test chamber; (a) injection, (b) evaporation and distribution under continuous monitoring, and (c) test commencement.

S5. Calibration of the gas sensor

In the adsorption parameter calculations via adsorption-diffusion equation, a linear relationship between target molecule concentration at the surface of the sensor pellet and the sensor response level is assumed. This relationship, called the static characteristics of the sensor, in all chemoresistive gas sensors is nonlinear. This shortcoming is partly removed by arranging the target gas concentrations in the test chamber and design parameters of the microchannel so that the contamination level at the sensor pellet surface remains in low levels throughout the test. In this way, the mentioned relationship is approximately linear.

The static response of the sensor is plotted by measuring its response level when exposed to known levels of target molecule-contaminated atmospheres. Different concentrations of the target molecule are created in the test chamber using the method described in Section S4 which is also monitored with a reference sensor. The bare sensor is inserted in the chamber and time is allowed (1 min) for the sensor to reach its steady-state response. The response time of the sensor is ~ 20 s and 1 min is enough for steady response measurement. Sample results of sensor static response are represented in Figure S7, demonstrating approximate linearity up to a concentration level of ~200 ppm. Above 250 ppm the departure from linearity is significant. Based on these results, the system operation had to be arranged so that the target gas concentration in the microcavity never exceeds 200 ppm throughout the tests. The slope of the linear segment of the static characteristics of the sensor is used in the mathematical work carried out on the recorded response profiles. The static response of the sensor is regenerated every fortnight. Although the sensor nonlinearity is avoided by this technique, still the sensor nonlinearity is a major precision limiting feature of the present system. Indeed, regardless of many positive features, metal oxide sensors are by no means optimum for this application; using optical sensors are anticipated to solve this problem.

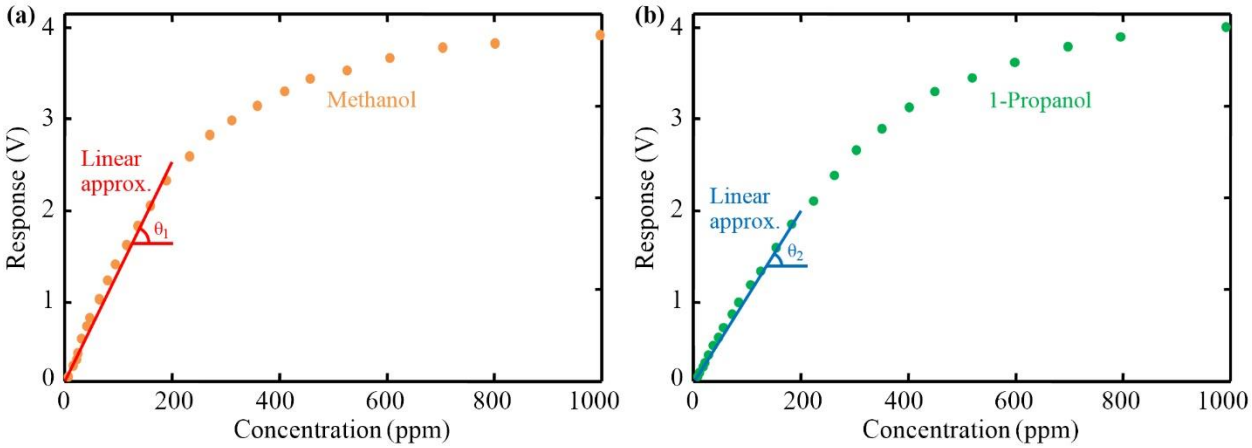

Figure S7. The static characteristics of the utilized sensor, recorded for methanol and 1-propanol. In both cases, a linear relationship approximately fits the results up to 200 ppm gas concentration.

S6. Repeatability and reproducibility of the measurements

Figure S8a-c shows the data obtained from PMMA, ZnO, and Au microchannels in 10 repeat tests. The error level in α values calculated from these diagrams is below 5%. Several microchannels of each type have been fabricated to examine the reproducibility of the results; the respective response profiles are given in Figure S9a-b. The α-values obtained from the many Au-coated microchannels differ within 10%. The same is true for the case of uncoated PMMA channels. However, α-values obtained from the plurality of ZnO-coated microchannels vary by ~30%. This larger variation is understood based on the differences in the thickness, morphology, and porosity of thick films produced by the drop-casting method, which render layers different in their surface properties.

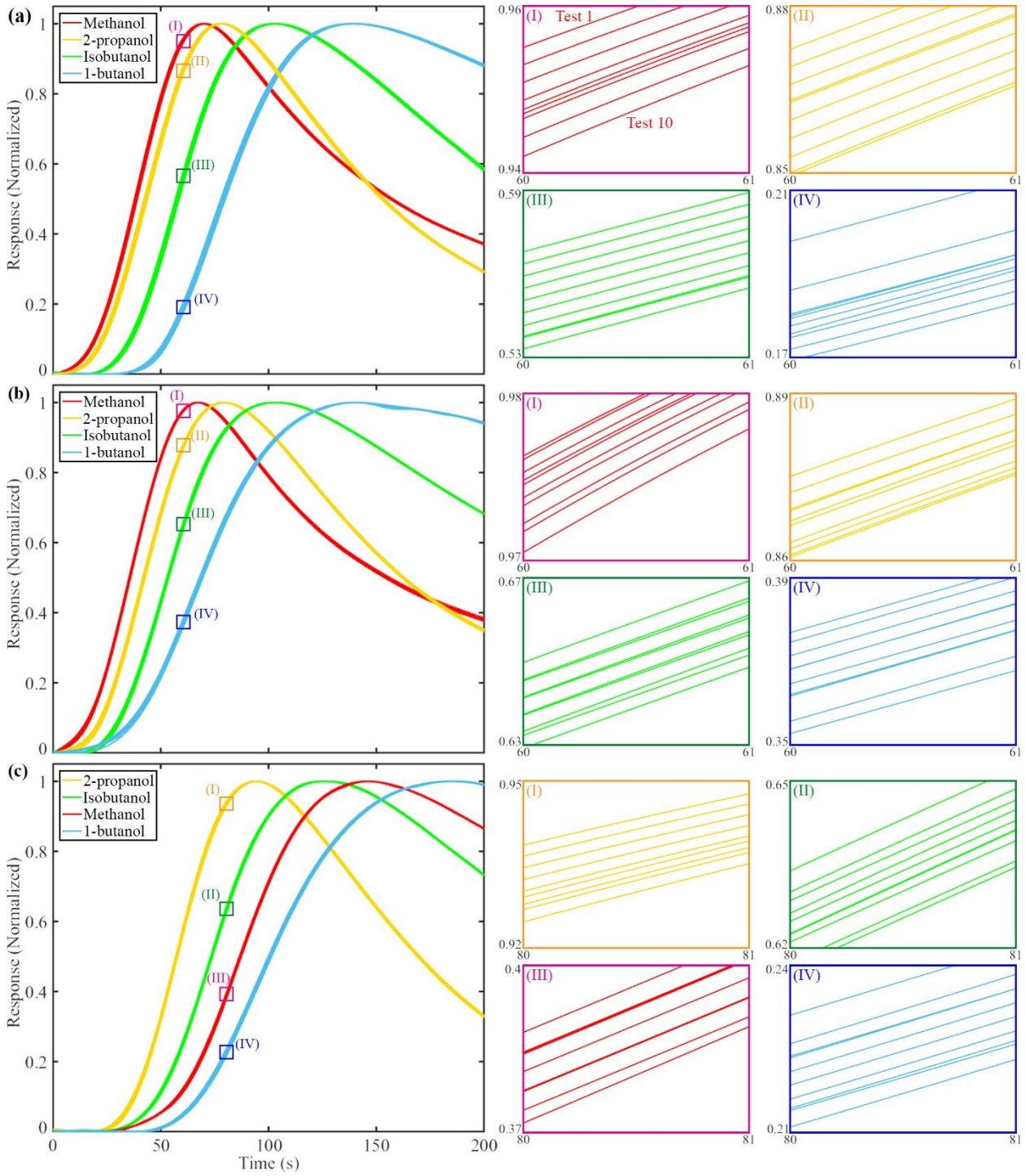

Figure S8. Response profiles obtained in 10 times repeated tests to demonstrate the repeatability of the adsorption-diffusion experiments performed for the stated target molecules through the uncoated (a), Au-coated (b), and ZnO-coated microchannels. The insets (I)-(IV) in each frame magnify the respective diagrams. The obtained response profiles are close so that the calculated α-values vary within 5%.

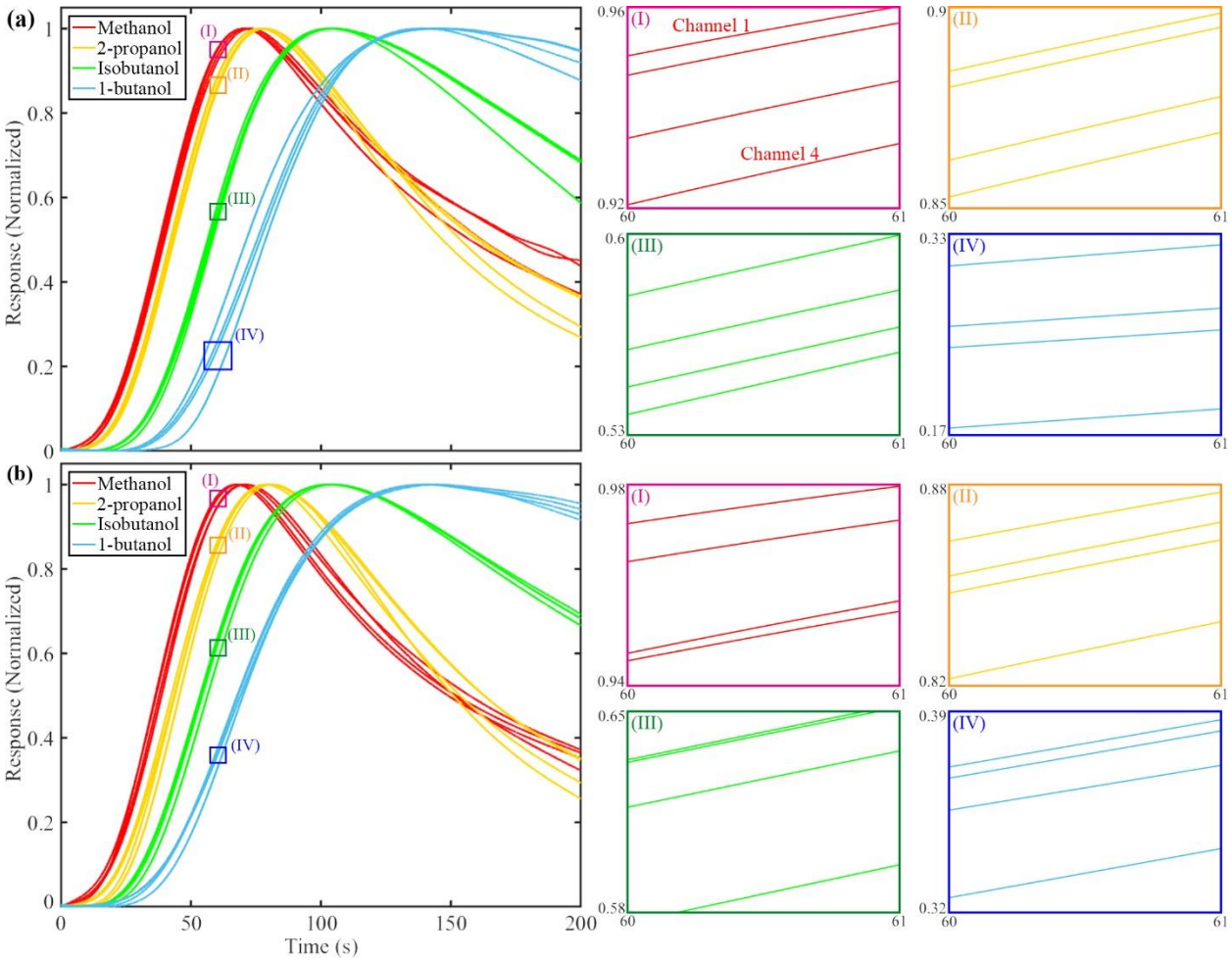

Figure S9. Response profiles obtained for the adsorption-diffusion of the stated target molecules in **(a)** four similarly produced PMMA microchannels, and **(b)** four similarly produced Au-coated microchannels. The α-values extracted from the data of intended similar samples varied within 10%.

S7. Measurements on small molecule gases

The surface interaction of small molecule gases, using the standard techniques, are examined at low temperatures close to their boiling points. Mainly due to the fact that the interactions of such molecules with solid surfaces are instantaneous and hard to evaluate. Although the microchannel geometry amplifies the effects of these interactions, the system is still incapable to detect the minor possible differences between different solid surfaces in interacting with gas molecules such as H_2 and CO. For examining this incapability, these gases are tested using the developed microchannels with different channel wall coatings.

The results are given in Figure S10a-b, showing that their flight time through the microchannel is almost independent of the coating material.

Detecting surface interactions with these gases may become possible via two different strategies: A) by decreasing the channel temperature to the boiling temperature of the target gas, B) by decreasing the channel depth to the submicron range which is expected to increase the sensitivity to the interaction differences by two orders of magnitude. None of these approaches are feasible on the present device. Further work on either of the approaches may prove fruitful.

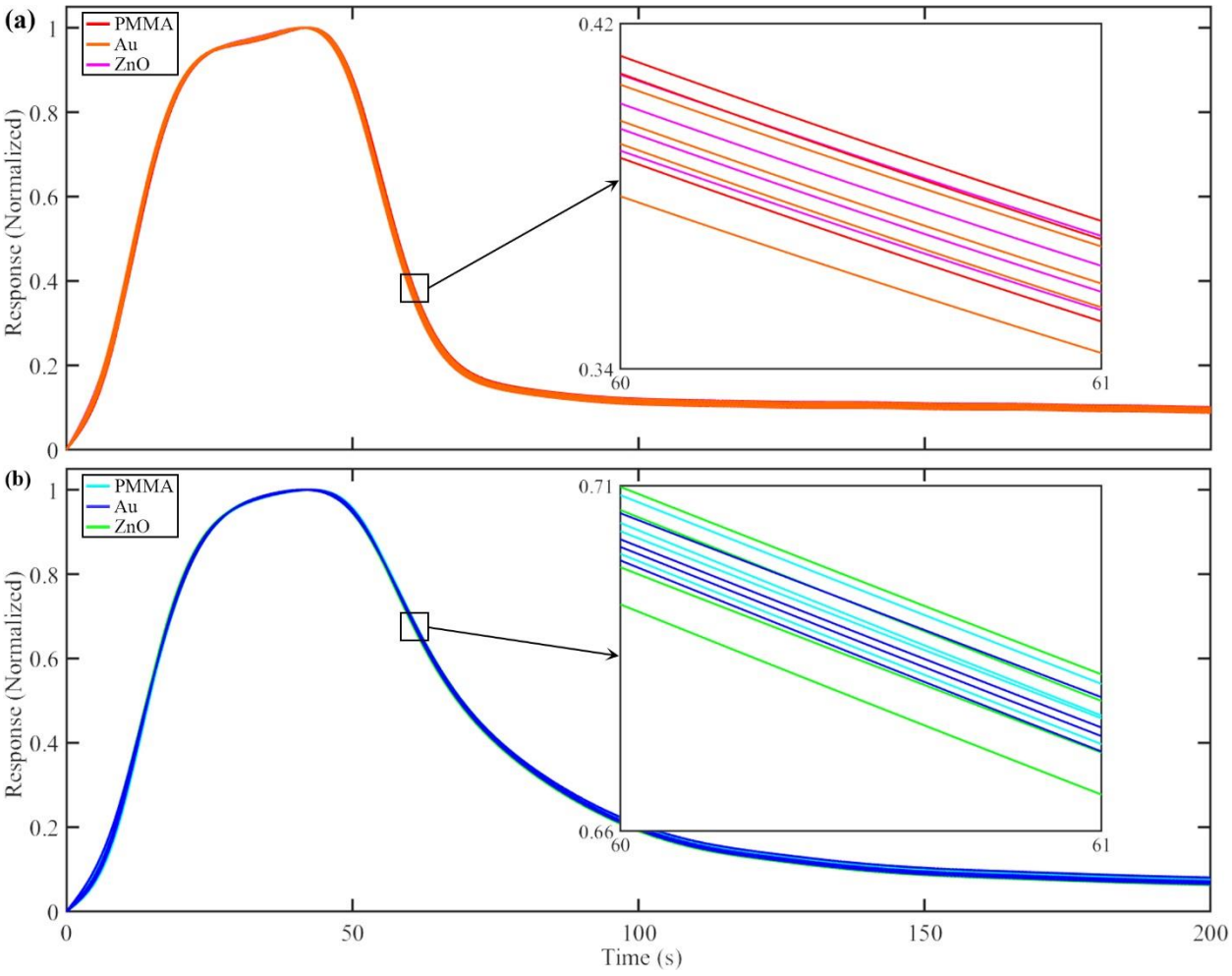

Figure S10. Response profiles recorded for the adsorption-diffusion of H_2 (a) and CO (b) in the stated microchannels showing overlapping of all test runs performed in the three different channel materials.

The temporal differences clearly observed in (a) and (b) are explained based on the difference in the diffusivity of the two target gases rather than their different adsorption tendencies.

In the cases of inert or chemically passive molecules such as Ar, CO_2, and N_2, the system encounters an additional problem, as the metal oxide sensors are insensitive to the presence of these molecules. Approach to these gases would require sensor replacement. For instance, an infrared gas detector can be utilized to measure the presence of CO_2 at the microchannel end.